to appear in Journal of Climate

Sea ice response to wind forcing from AMIP models

C. M. Bitz [1], John C. Fyfe [2], and Gregory M. Flato [2]

Abstract. The arctic surface circulation simulated by atmospheric general circulation models is assessed in the context of driving sea ice motion. A sea ice model is forced by geostrophic winds from eight models participating in the Atmospheric Model Intercomparison Project (AMIP), and the results are compared to simulations with the sea ice model forced by observed winds. The mean sea level pressure in the AMIP models is generally too high over the Arctic Ocean, except in the Beaufort and Chukchi Seas, where it is too low. This pattern creates anomalous winds that tend to transport too much ice away from the coast of Greenland and the Canadian Archipalego, and into the East Siberian Sea, producing a pattern of ice thickness in the Arctic that is rotated by roughly 180° relative to what is expected based on observations. AMIP winds also drive too little ice transport through Fram Strait and too much transport east of Svalbard by way of the Barents Sea. These errors in ice thickness and transport influence ice growth and melt rates and hence the freshwater flux into the ocean. Sensitivity experiments show the ice responds primarily to the climatological mean annual cycle of the geostrophic winds. Daily wind variability is necessary to create sufficient ice deformation and open water, but the sea ice response is rather insensitive to the details of the daily variations.

1. Introduction

Sea ice components of coupled climate models are increasing in complexity in an attempt to improve high latitude climate simulations. Many models now include more sophisticated solutions of the ice momentum equation and some even represent the subgrid scale distribution of sea ice thicknesses [e.g., Flato et al., 2000; Bitz et al., 2001]. These sea ice model improvements will be effective only if the atmosphere and ocean component models provide accurate forcing. Wind forcing is particularly important for transporting and deforming sea ice and creating open water. However, analysis of arctic atmospheric surface circulation patterns suggest serious biases exist in many Atmospheric General Circulation Models (AGCMs) [Walsh and Crane, 1992; Bromwich et al., 1994]. When ice transport is allowed, these biases may lead to unrealistic ice thickness patterns. As an example, Weatherly et al. [1998] show a highly unrealistic sea ice thickness pattern, with ice build-up in excess of 10 m in the East Siberian and Chukchi Seas.

In this study we examine the response of a particular sea ice model to winds from eight AGCMs participating in the Atmospheric Model Intercomparison Project (AMIP) [Gates, 1992]. The results are compared to simulations with the sea ice model forced by winds from two atmospheric reanalyses. In this way we assess the arctic atmospheric surface circulation in the context of driving sea ice motion. AMIP models employ realistic surface conditions, and therefore we have some confidence that the errors in the atmospheric circulation are not dominated by inaccuracies in the sea ice state. However, the AMIP sea ice surface boundary conditions are rather crude and they vary among models.

2. Forcing data and sea ice model

The names and countries of origin for the two reanalyes and eight AMIP models used in this study are given in Table 1. The AMIP models use prescribed monthly mean sea surface temperature (SST) and sea ice extent for the period 1979-1988. Two of the AMIP models prescribe surface temperature for sea ice covered regions from climatology and the remaining six compute surface temperature based on prescribed sea ice thickness and lead fraction (see Table 2). Among those that compute the ice surface temperature, some assume a spatially and temporally variable thickness field and lead fraction, while others fix the thickness at a constant value and assume the local ice cover is either 0 or 100%. The resolution and model physics of AMIP models varies, as summarized in Table 3. More information about the AMIP models is available in the

[1] Polar Science Center, University of Washington
[2] Canadian Centre for Climate Modelling and Analysis, University of Victoria

Table 1. Full names and country of origin for the two reanalyses and eight AMIP models used in this study.

Model	Full Name	Country
ERA	European Centre for Medium-Range Weather Forecasts Reanalysis	England
NCEP	National Centers for Environmental Prediction Reanalysis	United States
BMRC	Bureau of Meteorology Research Centre	Australia
CCC	Canadian Centre for Climate Modelling and Analysis	Canada
CSIRO	Commonwealth Scientific & Industrial Research Organization	Australia
CSU	Colorado State University	United States
ECMWF	European Centre for Medium-Range Weather Forecasts	England
MRI	Meteorological Research Institute	Japan
RPN	Recherche en Prévision Numérique	Canada
UGAMP	The UK Universities' Global Atmospheric Modelling Programme	England

Table 2. Sea ice boundary conditions for the two reanalyses and eight AMIP models.

Model	Ice Surface Temperature	Thickness	Lead Fraction
ERA	Prescribed Climatology	N.A.	N.A.
NCEP	Prognostic	Uniform 2 m	0
BMRC	Prognostic	Uniform 2 m	0
CCC	Prognostic	Nonuniform	Nonuniform
CSIRO	Prognostic	Uniform 2 m	0
CSU	Prognostic	Uniform 1.5 m	0
ECMWF	Prescribed Climatology	N.A.	N.A.
MRI	Prognostic	Nonuniform	Nonuniform
RPN	Prognostic	N.A.	N.A.
UGAMP	Prescribed Climatology	N.A.	N.A.

N.A. indicates not applicable
Nonuniform indicates spatially and temporally variable prescribed fields

Table 3. Resolution, orography, and gravity wave drag scheme in the two reanalyses and the eight AMIP models. Noting only orography smoothing procedures more complex than the area-averaging of orographic heights over model grid boxes and/or the truncation of spectral representations of orography at grid resolution are tracked here.

Model	Resolution Horizontal[1]	Resolution Vertical	Orographic Smoothing	Gravity Wave Drag
ERA	T106	31	envelope	Palmer et al. [1986]; Miller et al. [1989]
NCEP	T62	28		Alpert et al. [1988]
BMRC	R31	9	Cressman	Palmer et al. [1986]
CCC	T32	10		McFarlane [1987]
CSIRO	R21	9		Chouinard et al. [1986]
CSU	4°x5°	17	subjective	
ECMWF	T42	19	envelope	Palmer et al. [1986]; Miller et al. [1989]
MRI	4°x5°	15		Palmer et al. [1986]; Yagai and Yamazaki [1988]
RPN	T63	23		McFarlane [1987]
UGAMP	T42	19	envelope	Palmer et al. [1986]

1. T=triangular and R=rhomboidal spectral truncation
2. Cressman = area-averaged weighting function with a 3° radius of influence [Cressman, 1959]

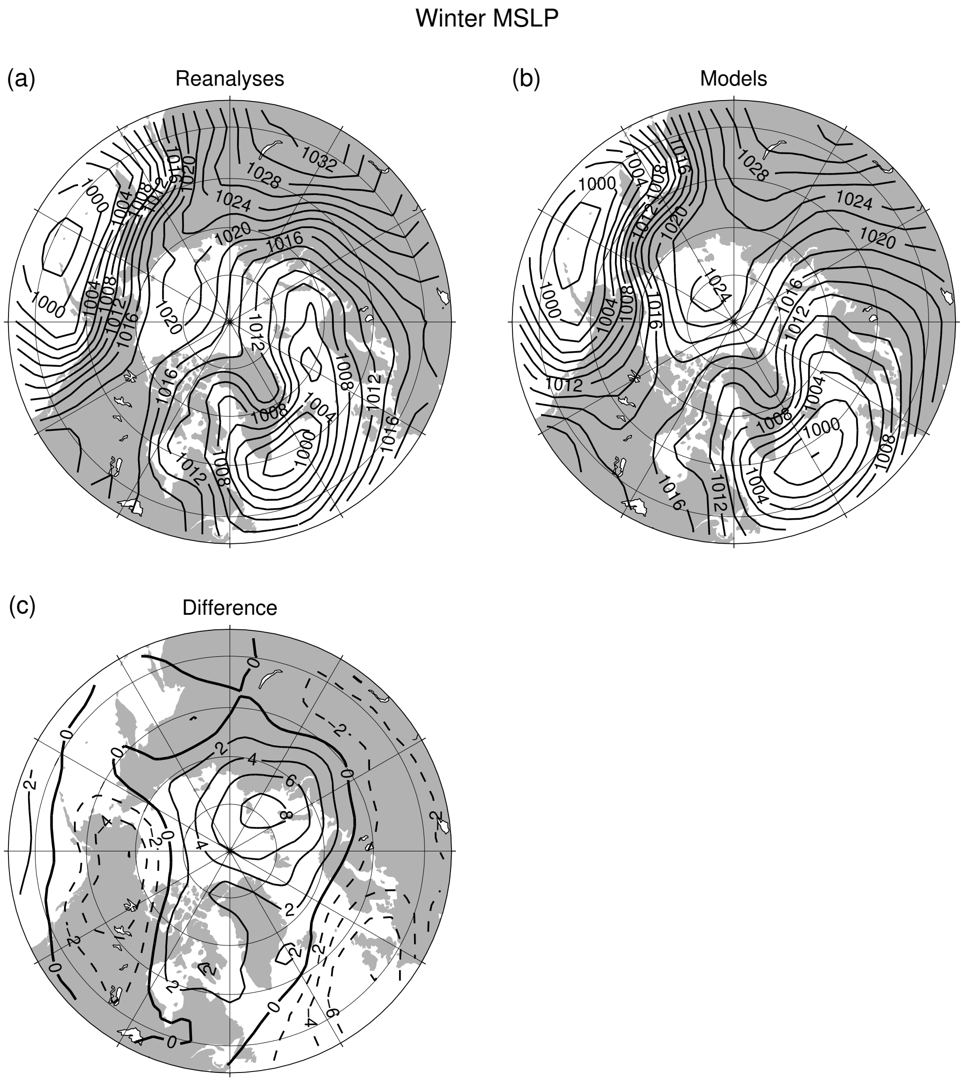

Figure 1. The winter (December-February) mean sea level pressure field in millibars averaged over (a) the ERA and NCEP reanalyses, (b) the eight AMIP models, and (c) their difference.

report by Phillips [1994].

The sea ice model used for this study is a two-category, dynamic-thermodynamic model, on an 80-km Cartesian coordinate grid of the Arctic Ocean and northern most portions of the Pacific and Atlantic Oceans. Sea ice velocity is computed from the equation of motion for a material with a viscous-plastic rheology [Hibler, 1979] using the efficient numerical method of Zhang and Hibler [1997]. The vertical temperature profile is resolved in the ice and snow with an explicit brine-pocket parameterization from the study of Bitz and Lipscomb [1999]. The sea ice overlies a slab mixed layer model with constant ocean currents and heat flux from the deep ocean prescribed from a coupled ice-ocean general circulation model by Hibler and Zhang [1993].

In an effort to isolate the response to the atmospheric surface circulation alone, only the geostrophic winds from the AMIP models and reanalyses are used to force the sea ice model. The AMIP model and reanalysis sea level pressure data were truncated to T31 resolution, transformed to a common 96x48 point Gaussian grid, and then interpolated to the 80-km sea ice model grid.

In all simulations, the 2-m air temperature is prescribed for the AMIP period from the Polar Exchange at the Sea Surface (POLES) dataset, which is computed from surface air temperature observations obtained from buoys, manned drifting stations, and meteorological land stations [Rigor, 2000]. Incoming longwave irradiance is parameterized from Maykut and Church [1973] as a function of air temperature, a constant 85% relative humidity, and a cloud climatology from Russian drifting stations (R. Colony, personal

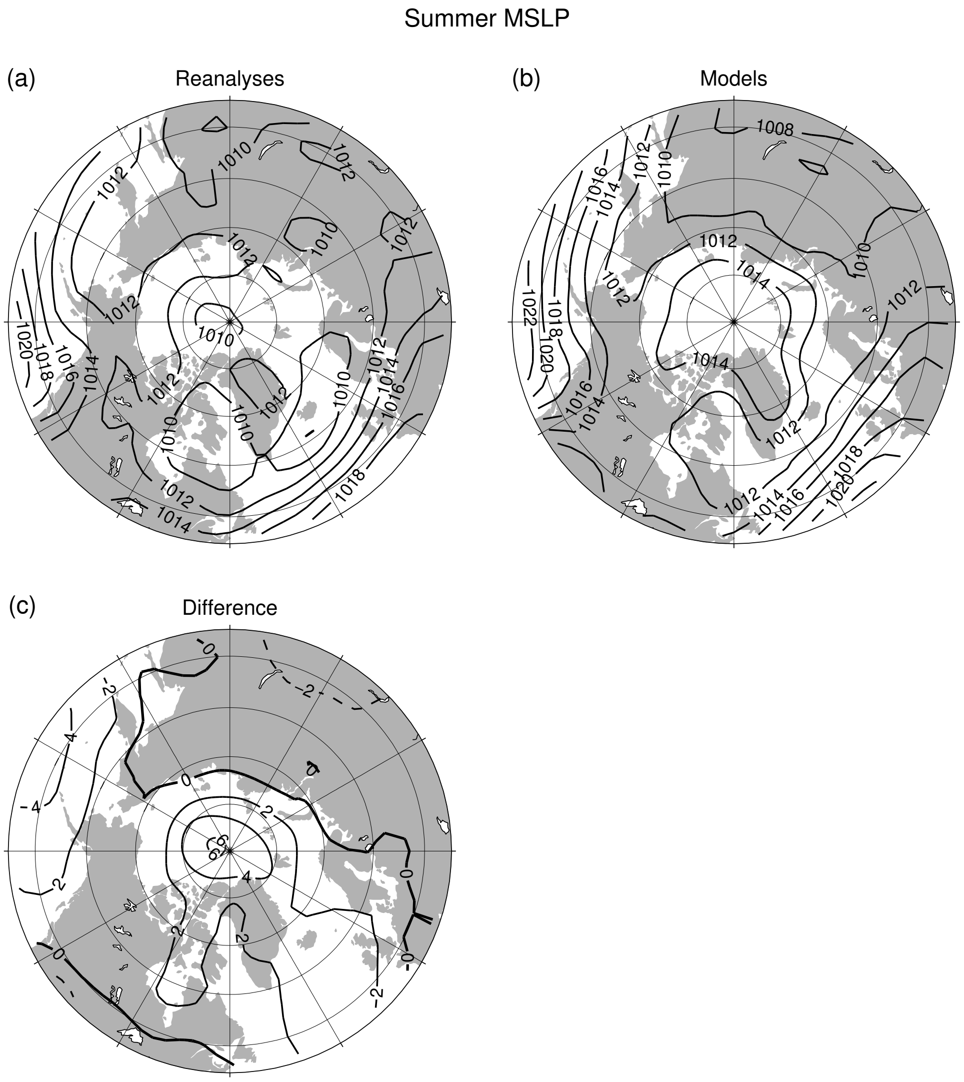

Figure 2. Same as in Figure 1 but for summer (July-September).

communication). Incoming shortwave radiation is parameterized by multiplying the clear sky empirical equation from Zillman [1972] by a cloudiness factor from Laevastu [1960]. Snowfall is prescribed from Maykut and Untersteiner [1971] and is annually periodic. Sensible and latent heat fluxes are parameterized from standard bulk aerodynamic formulae. The model is integrated with wind and air temperature forcing from the period 1979-1988 over two cycles: The first serves as a spinup and the second is used for analysis. The daily input data are linearly interpolated to the model timestep, which is 6 hours.

3. Atmospheric surface circulation in the reanalyses and AMIP models

In winter (December-February) the reanalysis 1979-1988 mean sea level pressure (MSLP) is characterized by a ridge extending from Siberia to North America through the Beaufort Sea (see Figure 1a). The Icelandic low extends into the Norwegian and Barents Sea, forming another prominent arctic surface feature. The resulting geostrophic winds drive sea ice motion that on average exhibits an anticyclonic Beaufort gyre, a general drift from the Siberian Arctic towards Greenland, through Fram Strait, and out to the northern North Atlantic. Summertime (June-August) MSLP gradients are weak compared to winter and there is a very weak low pressure center near the North Pole (see Figure 2a).

The AMIP models, averaged over the same period,

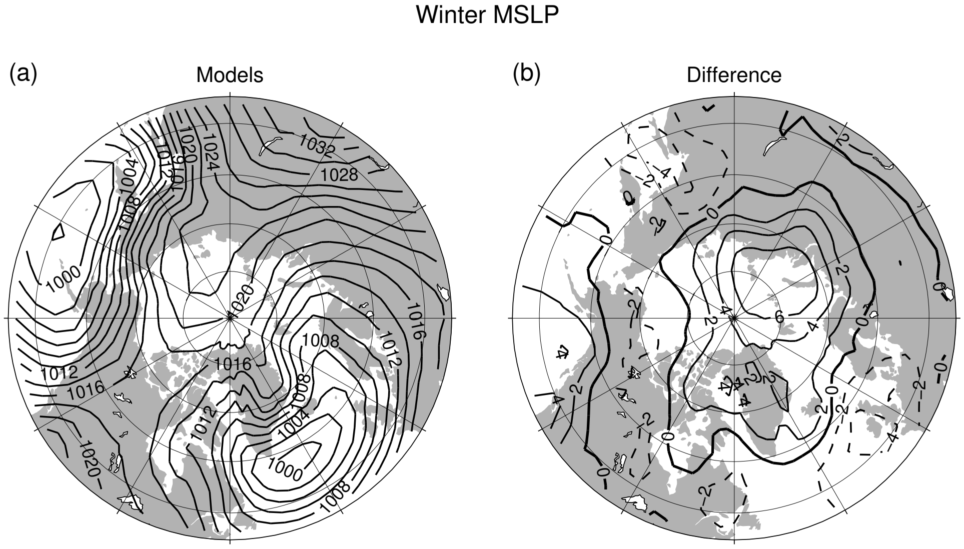

Figure 3. The winter (December-February) mean sea level pressure field in millibars averaged (a) from six CMIP models and (b) their difference from the reanalyses in Figure 1a.

appear to capture the major features of the wintertime circulation (see MSLP averaged across the AMIP models in Fig. 1b). However closer inspection indicates that the Icelandic low does not penetrate far enough into the Arctic. The MSLP difference between models and reanalyses (Fig. 1c) clearly shows a high pressure bias over most of the Arctic Basin, especially over the Kara Sea, and a low pressure bias over northwestern North America. This pattern creates an unrealistically strong northeasterly geostrophic wind in the Chukchi Sea, which has severe consequences for sea ice build up in the East Siberian Sea, as we will see in section 4.

Summertime MSLP among AMIP models is on average too high over the entire Arctic (see Fig. 2b and c). None of the AMIP models reproduces the closed low centered near the North Pole that is present in the reanalyses and in the POLES geostrophic wind data sets (not shown). The sea level pressure is biased generally high over all mid- and high-latitude ocean covered surfaces.

Lambert et al. [2000] used a cyclone and anticyclone tracking method to analyze the day to day behavior in thirteen AMIP models. Consistent with the pattern shown in Fig. 1, they found models typically have an abundance of cyclones in northwestern North America and an abundance of anticyclones in the Laptev and Kara Seas region.

We digress momentarily to examine the mean sea level pressure from the last 10 years of integration from six Coupled Model Intercomparison Project (CMIP) models to determine whether coupled models have similar surface circulation problems. Some differences between the CMIP and AMIP surface circulation are to be expected because some of the models are from different institutions and most CMIP models are later generation models. Furthermore the AMIP models were integrated using boundary forcing from a specific decade (1979-1988), while the CMIP models freely develop their own surface conditions. Figure 3 shows the winter MSLP averaged across the CMIP models and the difference from the mean of the ERA and NCEP reanalyses. The patterns are very similar to those in Fig. 1b and c. Therefore we can rule out the possibility that common errors in AGCM surface circulation are isolated to uncoupled models.

We also compared the arctic surface circulation in the CCC AGCM integrated with three different surface conditions. The first uses prescribed SST and sea ice extent (i.e., the AMIP integration described in section 2). In the other two integrations, the AGCM is coupled to a full ocean and sea ice model, but in one the sea ice is constrained to be motionless (i.e., thermodynamic only sea ice with a lead fraction computed as a function of the ice thickness), and the other includes a realistic sea-ice dynamics component [Flato et al., 2000]. All three integrations produce similar arctic MSLP (not shown). Details of the sea ice distribution and thickness do not seem to be a crucial factor in determining MSLP errors.

4. Comparison of sea ice response to AMIP model forcing

To illustrate the role of the circulation errors discussed above, we force a sea ice model with geostrophic winds from the eight AMIP models and two reanalyses. We begin our analysis by examining the ice thickness pattern for April and September, roughly the maximum and minimum of the annual cycle, (see Figs. 4 and 5)

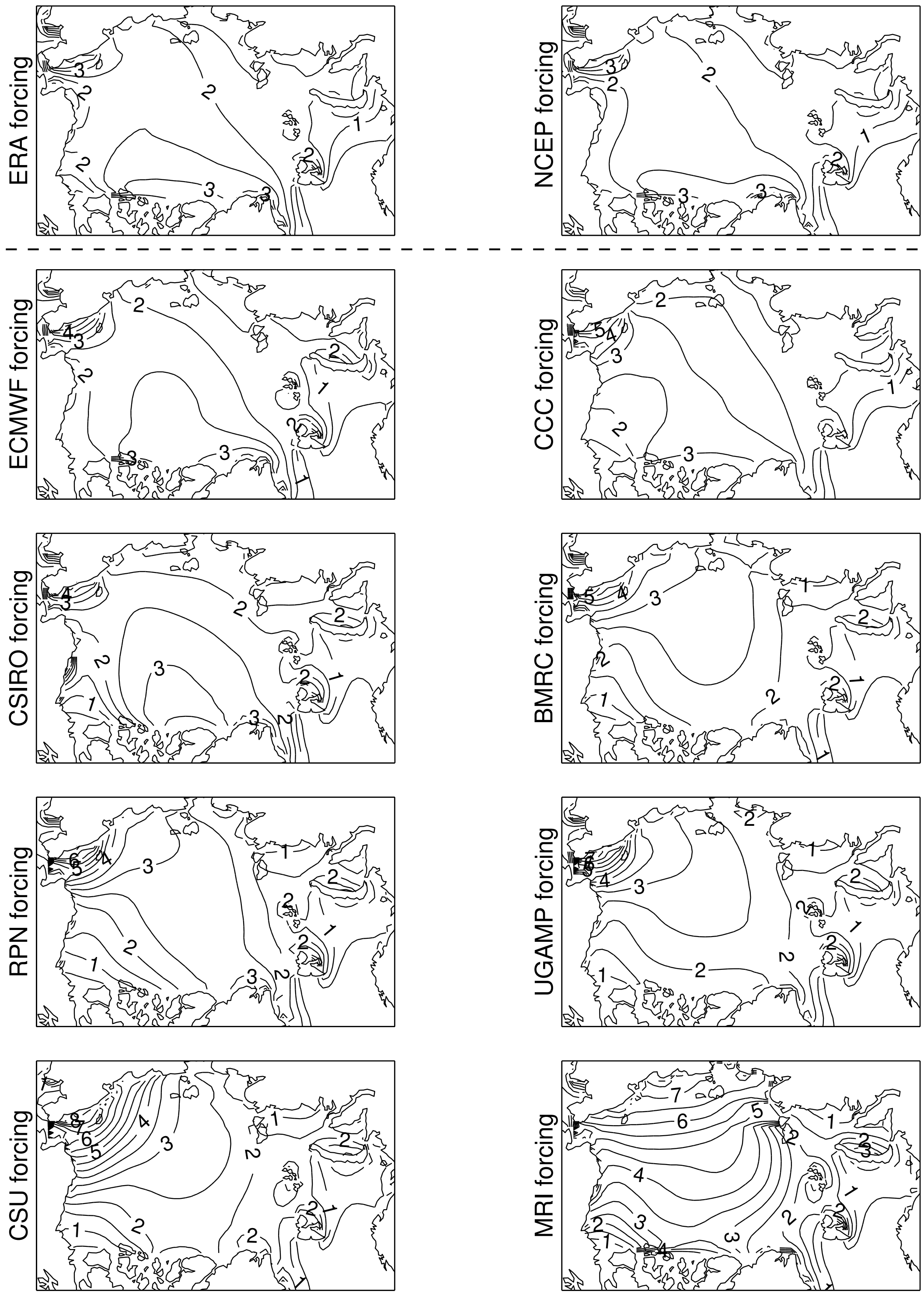

Figure 4. April mean simulated ice thickness for a sea ice model forced with two reanalyses and eight AMIP models. The later eight integrations are ordered roughly according to how successfully they compare to the simulations forced with reanalysis winds.

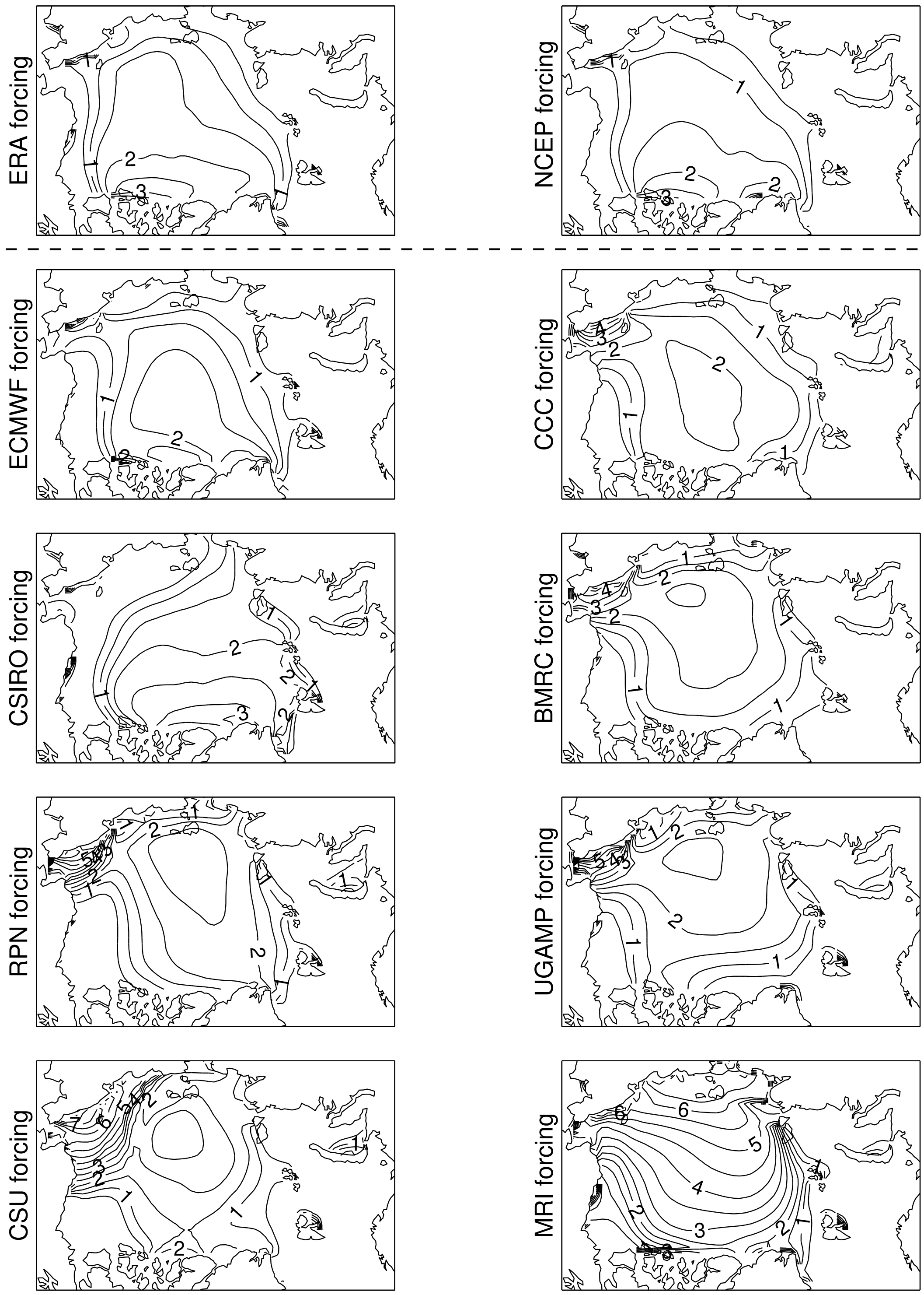

Figure 5. Same as in Figure 4 but for September.

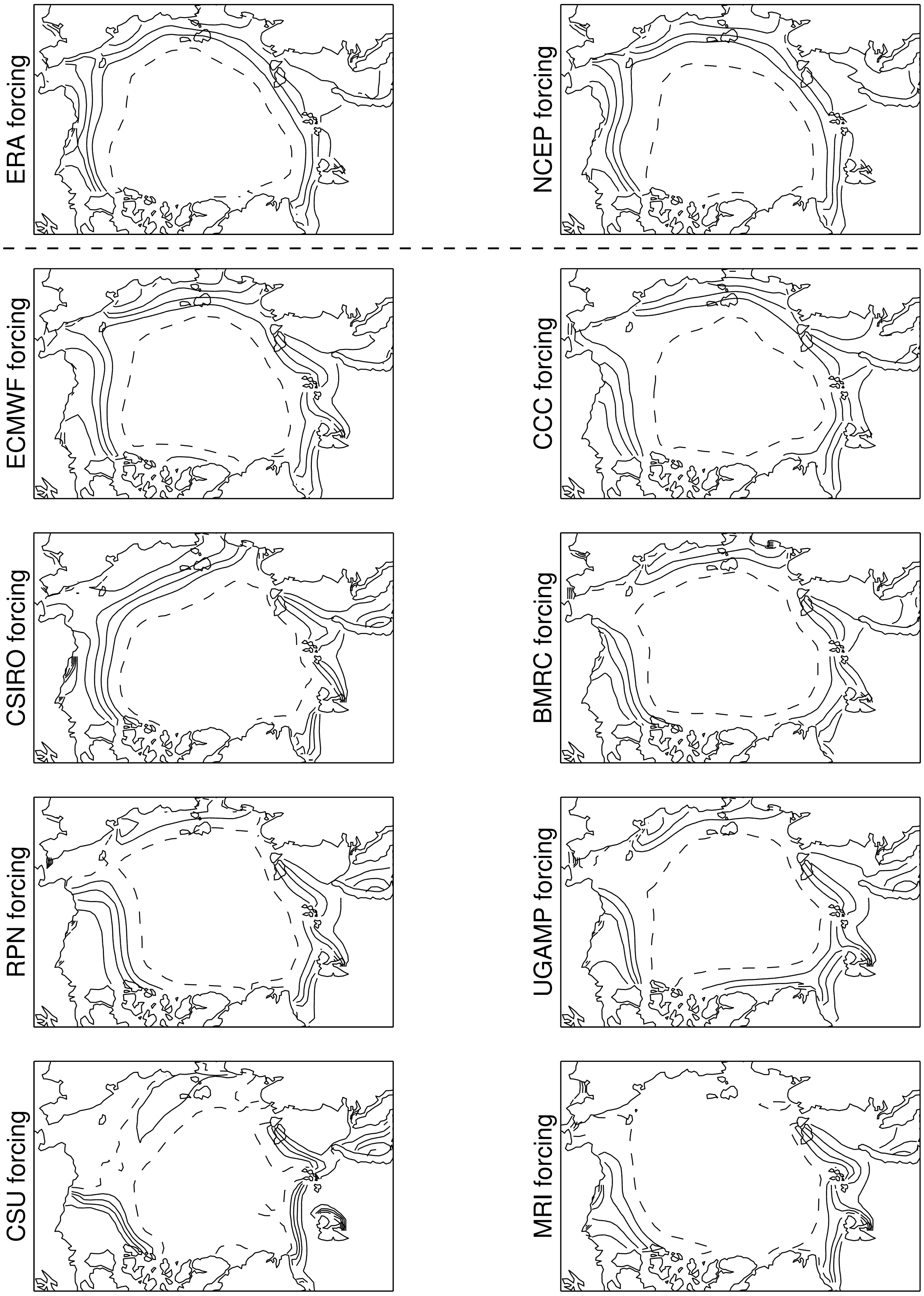

Figure 6. Same as in Figure 5 but for ice concentration. Dashed line indicates 90% and solid lines indicate 10–70% in 20% increments.

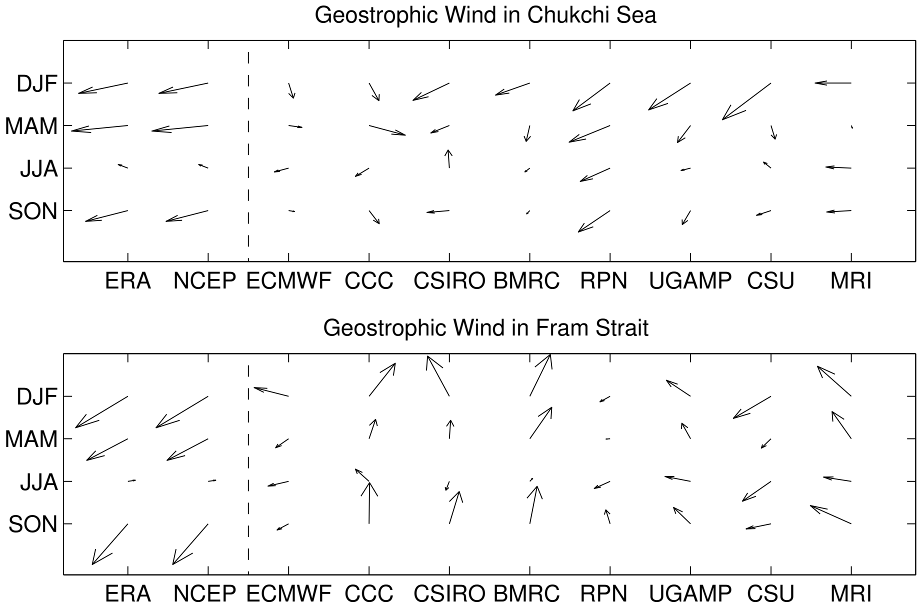

Figure 7. Seasonal average geostrophic winds in the Chukchi Sea and Fram Strait. The reanalysis winds are shown to the left of the dashed lines and the difference between the AMIP model and the mean of the reanalysis winds are shown to the right. The meridional (zonal) component is parallel to vertical (horizontal) axis.

and the September ice concentration (see Fig. 6).

The two reanalysis data sets differ somewhat in their estimates of MSLP and this leads to a modest difference in sea ice patterns (upper 2 panels of Figs. 4–6). In both cases, the spatial patterns are in broad agreement with observational estimates [e.g., Bourke and Garrett, 1987; Gloerson et al., 1992], especially the pattern of thicker ice on the North American side of the basin and thinner ice on the Siberian side. Although the climatological ice thickness is poorly known, the ice thickness appears to be biased low in the central Arctic and especially north of Greenland and the Canadian Archipalego, which is common in simulations with two-category models. Nevertheless, the simulation with observationally based forcing provides a sufficiently realistic comparison for the results described below. The thickness and compactness patterns that are forced by AMIP model output share some common errors that range in severity. AMIP model winds tend to drive too much ice into the East Siberian Sea and not enough north of Greenland and the Canadian Archipalego. Among the worst cases in Figs. 4 and 5, the pattern of ice thickness in the Arctic is rotated by roughly 180° relative to what is expected, with the thickest ice north of Siberia and thinner ice on the North American side. One consequence of this excessive build-up is the lack of a proper summertime melt back in the Chukchi Sea.

The thickness and compactness patterns for the CSIRO case are unusual among the integrations. The moderate build up of ice in the East Siberian Sea during winter is reversed in summer by anomalously strong southerly winds in the Chukchi Sea.

The seasonally averaged geostrophic winds from the AMIP models and reanalyses in the Chukchi Sea (see Fig. 7a) indicate that most of the models have an anomalous northerly and/or easterly component. The AMIP models whose winds produce a sea ice response in the Chukchi Sea in best agreement with the reanalysis results (e.g., ECMWF and CCC cases) have anomalous winds that are small and vary in direction throughout the annual cycle. Interestingly only these models have significant anomalous westerly winds in any season. The poorest simulations come about from persistent wind errors. The unusual summertime southerly winds in the CSIRO model are also apparent.

Sea ice export west of Svalbard, through Fram Strait, is a key component of the freshwater transport between the Arctic Ocean and the northern North Atlantic [Aagaard and Carmack, 1989]. Also the sea ice cover in the subpolar seas influences the heat balance by modulating air-sea heat exchange and by latent heat storage. Modeling studies have shown that the freshwater and heating supplied by sea ice influences convection in the northern branch of the Atlantic Ocean thermohaline circulation [Yang and Neelin, 1993; Zhang et al., 1995; Lohmann and Gerdes, 1998].

Figures 8a and b show the modeled sea ice export west and east of Svalbard for all ten simulations. Figure 8c shows the net export from both sides of Svalbard averaged over the two reanalyses and the eight AMIP model cases, along with an estimate of the 1990-1995 mean export through Fram Strait based on observations

[Kwok and Rothrock, 1999]. Observational estimates of ice export vary from 0.038 to 0.12 Sv, in part due to large interannual variability but also due to uncertainty in the measurements and assumptions used. It is typical for low-resolution, two-category sea ice models to predict values that are at the low end of this range because the ice being exported is too thin and the ice velocity through the strait is not well resolved. Some models also tend to erroneously transport ice on the east side of Svalbard, where observations show no substantial transport. If we include export on both sides of Svalbard (i.e., net ice export), the reanalysis cases predict about 23% less sea ice export than was estimated by Kwok and Rothrock [1999].

Generally the response to AMIP winds qualitatively reproduces the mean annual cycle of export, but an even greater fraction of the net export occurs east of Svalbard than in the cases forced with reanalysis winds. The net export averaged over the AMIP wind-driven cases is 24% less than the average over the reanalysis wind-driven cases. The wind vectors in Fig. 7b indicate that the AMIP models have anomalous southerly and/or easterly flow during the cold season (i.e., insufficient northerly flow driving ice export, see Fig. 1).

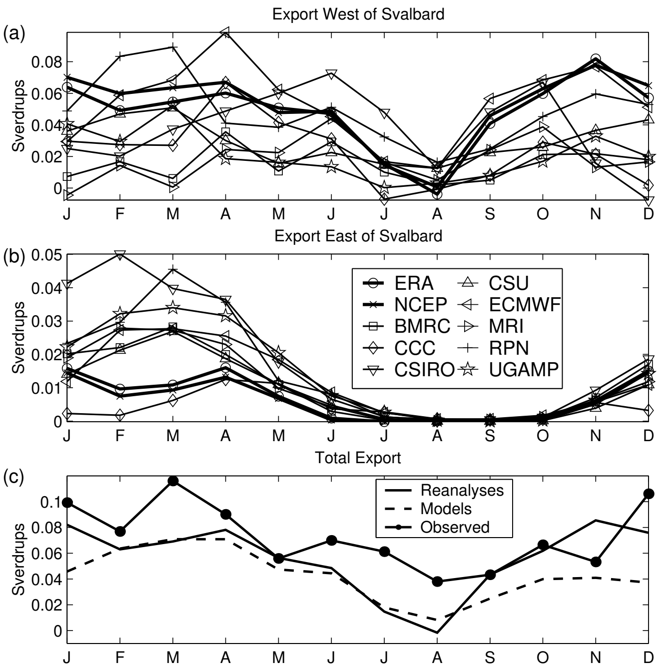

Figure 8. Sea ice export (a) east and (b) west of Svalbard and (c) total export. (1 Sverdrup = 10^6 m^{3}s^{-1})

A measure of the sea ice contribution to the oceanic freshwater flux is the annual total of growth minus melt, termed the net freezing rate [e.g., Steele and Flato, 1999]. Although the net freezing rate is a key component of the freshwater budget of the high latitude ocean, there is no way to measure it directly. According to Steele and Flato [1999], the net freezing rate estimated by a variety of sea ice models exhibit only rough agreement in most regions and models disagree even as to the sign in the Beaufort Sea. Here we compare an estimate of the net freezing rate from the integrations forced by reanalysis winds (Fig. 9a) with that averaged over the integrations forced by AMIP winds (Fig. 9b). The difference (Fig. 9c) indicates that the AMIP-forced results are comparatively low throughout most of the Arctic Basin, as expected because sea ice export out Fram Strait is also relatively low. The influence of AMIP winds steering too much ice to the east of Svalbard is manifested by more melting in the Norwegian Sea. Differences as high as 100 cm yr^{-1} occur where there is seasonal ice, indicating an excess of growth in the Beaufort Sea and excess melt in the Laptev Sea.

5. The respective roles of the annual cycle and daily variability

Earlier ice model studies [e.g., Flato and Hibler, 1992] demonstrated the importance of high-frequency (i.e., daily) variability in wind forcing for obtaining realistic mean ice motion and transport. Here we briefly explore the relative roles of the climatological annual cycle and daily variations of wind forcing produced by the AMIP models. For these experiments we choose the BMRC model as a representative sample (based on Figs. 4 and 5, it produces ice thickness results similar to the AMIP average).

For both the ERA reanalyses and the BMRC model we compute the climatological annual cycle of MSLP (the average daily values over the 10-year AMIP period) and smooth it with a 30-day running mean. Daily anomaly fields are computed as the daily field minus the climatological daily field. Geostrophic winds are computed from these pressure fields.

Figure 10 shows the simulated April ice thickness from wind forcing composed of a climatological annual cycle (denoted by an overbar) plus daily anomalies (denoted by a superscripted star) for all possible combinations of the ERA and BMRC forcings. In comparing these four cases, it is clear that the climatological mean annual cycle is the essential component that determines the sea ice thickness pattern. We repeated these experiments with the MRI model because its winds drive one of the most extreme patterns among those we studied. We do not show the results though, because the conclusion is the same. While the actual sea ice circulation differs on daily timescales, the monthly mean circulation (not shown) is very similar for cases forced by the same climatological mean wind.

An integration performed with ERA climatological winds only and no daily anomalies, produces a thickness pattern (not shown) that is nearly uniform, at 175 cm, across most of the Arctic Basin. There is a slight build up of ice north of the Canadian Archipalego, but

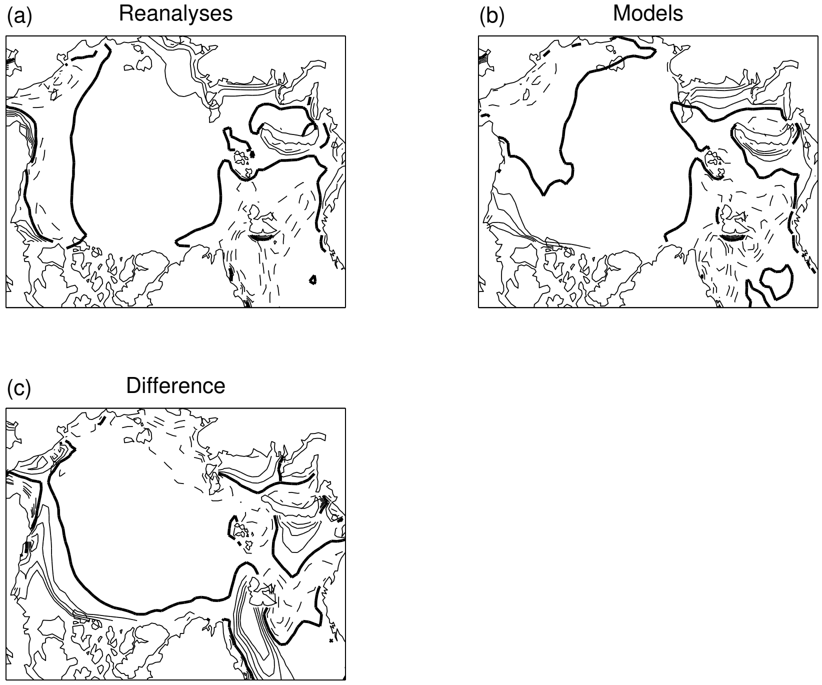

Figure 9. Simulated net freezing rate, which is equivalent to the annual total of growth minus melt, in centimeters per year averaged over 1979-1988. The fields are averaged for integrations forced by (a) ERA and NCEP reanalyses and (b) by the eight AMIP models, and (c) their difference. Negative values are dashed and indicate melt is greater than growth. Zero contour is heavy. Contour interval is 50 cm yr^{-1} in a–b, and 25 cm yr^{-1} in c.

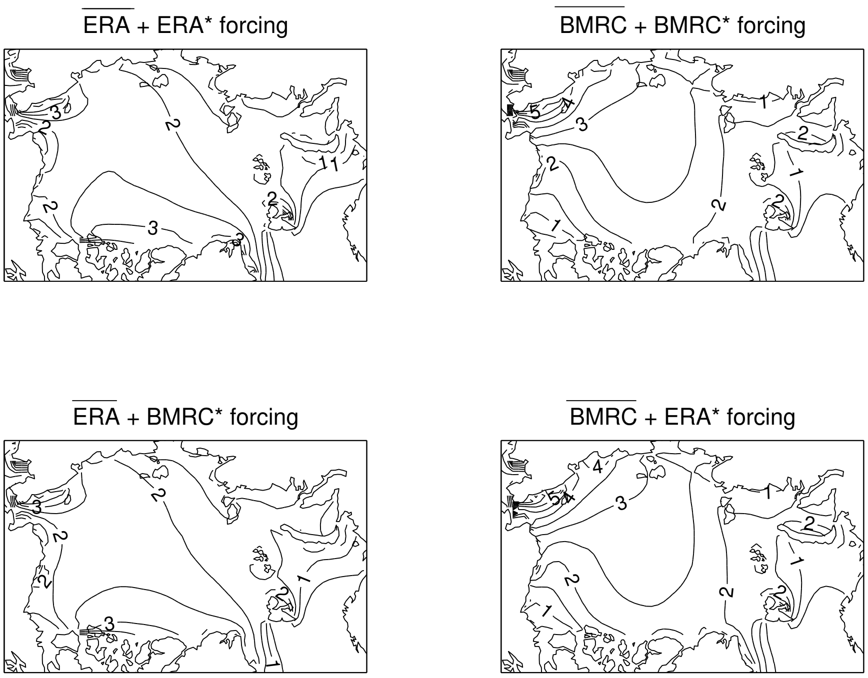

Figure 10. April sea ice thickness pattern when the ice model is forced by a combinations of winds from ERA or BMRC climatological mean annual cycle (denoted by overline) plus daily anomalies (denoted by superscripted star).

the maximum thickness is about 225 cm. In the absence of daily (synoptic-scale) winds, deformation is weak and very little open water develops within the ice pack during winter. Consequently, there is much less new ice growth over open water. Daily winds are also necessary to produce instantaneous forcing that is large enough to overcome the shear strength of the modeled ice pack [Flato and Hibler, 1992]. Yet the ice response is not very sensitive to the actual direction and amplitude of the daily anomalies.

6. Discussion

Identifying the features of the AGCMs that are essential for simulating the arctic surface circulation in the context of the sea ice response is an inviting but difficult exercise. Based on our sea ice simulations with AMIP winds, the ECMWF model winds produce the response most like the integration with reanalysis winds, and the CCC model is a close runner up. The ECMWF model has prescribed sea ice surface temperature that is annually periodic, while the CCC model computes sea ice surface temperature based on prescribed ice thickness and lead fraction (Tables 2). Furthermore, sea ice boundary conditions in the MRI model appear to be similar to that of CCC (Table 2), yet the sea ice model responds to winds from these two models in vastly different ways. The coupled model results mentioned in section 3 supports the evidence that sea ice boundary conditions are not a crucial factor.

Orographic effects, including their influence on gravity wave drag, may have a strong influence on the surface circulation in the Arctic. Momentum transport associated with unresolved orographically forced wave breaking and dissipation are parameterized with various gravity wave drag schemes as noted in Table 3. ECMWF and CCC models have different methods for orographic smoothing and wave drag, and hence nothing stands out as the key to their success. Furthermore, the UGAMP and ECMWF models share a common root and yet UGAMP winds are poor and ECMWF are quite good. The models differ primarily in their calculation of radiation, convection, surface fluxes, vertical advection, and lateral and vertical dissipation. It is necessary to perform sensitivity experiments to determine which of these features is responsible for the key differences.

Another potential influence on the surface circulation is model resolution (see Tables 3). Indeed the ECMWF model is one of the higher resolution models, but the CCC model is average-to-low. RPN is the highest resolution model, and the sea ice response to its winds are not noticeably better. Therefore at least for these models, resolution does not appear to play a clear role. MRI and CSU are the only finite difference models (i.e., nonspectral) in the set of eight and they drive very poor sea ice circulations.

7. Conclusions

We have assessed the surface circulation in eight AMIP models in the context of their success at driving sea ice motion. The mean sea level pressure in the AMIP models is generally too high over the Arctic Ocean and too low over the Beaufort and Chukchi Seas. These biases are associated with anomalous geostrophic winds that transport too much ice into the East Siberian Sea. Among the worst cases, the pattern of ice thickness in the Arctic Basin is rotated by roughly 180° relative to what is expected based on observations.

AMIP winds drive too little ice transport through Fram Strait and too much transport east of Svalbard by way of the Barents Sea. Within the Arctic Basin, differences in ice transport lead to differences in the location of net ice growth or melt. These differences are largest in the marginal ice zones.

The sea ice thickness pattern is primarily determined by the climatological mean annual cycle of the winds. Daily (synoptic-scale) winds are needed to create sufficient deformation and open water in the sea ice pack, but the response is not very sensitive to their magnitude or direction.

Comparing features of the various AMIP models, it was not apparent that any particular attribute is associated with the model's ability to produce a realistic surface circulation. We examined the mean sea level pressure in six CMIP models as well and found the biases are roughly the same as those in the AMIP models. The CMIP models include coupled sea ice and ocean components and are generally more recent models. We also looked at both coupled (with and without prognostic sea ice) and uncoupled integrations from one model and found that the sea ice state does not have a large influence on the surface circulation.

Sea ice plays an important role in the postive feedbacks leading to enhanced high-latitude warming in coupled climate model projections. Improvements are therfore being made to the sea ice components of many climate models, particularly by introducing more realistic treatments of sea ice dynamics. The results here indicate that biases in the arctic surface circulation produced by the atmospheric component of such climate models are a major source of error in the modeled ice thickness and transport patterns.

Acknowledgments. We thank R. Moritz, J. Walsh, and J. Weatherly for helpful suggestions. This work was completed while CMB was supported by a NOAA Climate and Global Change fellowship.

References

Aagaard, K. and E. C. Carmack, 1989: The role of sea ice and other fresh water in the Arctic circulation. *J. Geophys. Res.*, **94**, 14485–14498.

Alpert, J. C., M. Kanamitsu, P. M. Caplan, J. Sela, G. H. White and E. Kalnay, 1988: Mountain induced gravity wave drag parameterization in the NMC medium-range model. in *Proc. 8th Conf. Numerical Weather Prediction, Baltimore, MD, American Meteorological Society*, pp. 726–733.

Bitz, C. M., M. M. Holland, A. J. Weaver and M. Eby, 2001: Simulating the ice-thickness distribution in a coupled climate model. J. Geophys. Res., in press.

Bitz, C. M. and W. H. Lipscomb, 1999: An energy-conserving thermodynamic model of sea ice. *J. Geophys. Res.*, **104**, 15,669–15,677.

Bourke, R. H. and R. P. Garrett, 1987: Sea ice thickness distribution in the arctic ocean. *Cold Regions Sci. and Tech.*, **13**, 259–280.

Bromwich, D. H., R. Tzeng and T. Parish, 1994: Simulation of the modern arctic climate by the NCAR CCM1. *J. Climate*, **7**, 1050–1069.

Chouinard, C., M. Beland and N. McFarlane, 1986: A simple gravity wave drag parameterization for use in medium-range forecast model. *Atmos.-Ocean*, **24**, 91–110.

Cressman, G. P., 1959: An operative objective analysis scheme. *Mon. Wea. Rev.*, **86**, 293–297.

Flato, G. M., G. J. Boer, W. G. Lee, N. A. McFarlane, D. Ramsden, M. C. Reader and A. J. Weaver, 2000: The Canadian Centre for Climate Modelling and Analysis global coupled model and its climate. *Clim. Dyn.*, **16**, 451–467.

Flato, G. M. and W. D. Hibler III, 1992: Modeling pack ice as a cavitating fluid. *J. Phys. Oceanogr.*, **22**, 626–651.

Gates, W. L., 1992: AMIP: The Atmospheric Model Intercomparison Project. *Bull. Amer. Meteor. Soc.*, **73**, 1962–1970.

Gloerson, P., W. J. Campbell, D. J. Cabalieri, J. C. Comiso, C. L. Parkinson and H. J. Zwally, 1992: *Arctic and Antarctic sea ice 1978-1987: Satellite passive microwave observations and analysis*. NASA.

Hibler, W. D. III, 1979: A dynamic thermodynamic sea ice model. *J. Phys. Oceanogr.*, **9**, 815–846.

Hibler, W. D. III, and J. Zhang, 1993: Interannual and climatic characteristics of an ice ocean circulation model. in W. R. Peltier, editor, *Ice and the Climate System*, Vol. Series I, Vol.12, pp. 633–652. NATO ASI Series.

Kwok, R. and D. A. Rothrock, 1999: Variability of Fram Strait ice flux and North Atlantic Oscillation. *J. Geophys. Res.*, **104**, 5,177–5,189.

Laevastu, T., 1960: Factors affecting the temperature of the surface layer of the sea. *Comment. Phys. Math.*, **15**, 8–134.

Lambert, S. J., J. Sheng and J. E. Boyle, 2000: Winter cyclone frequencies in thirteen models participating in the Atmospheric Model Intercomparison Project AMIP. *J. Climate*, **X**, submitted.

Lohmann, G. and R. Gerdes, 1998: Sea ice effects on the sensitivity of the thermohaline circulation. *J. Climate*, **11**, 2789–2803.

Maykut, G. A. and P. Church, 1973: Radiation climate of Barrow, Alaska, 1962–66. *J. Appl. Met.*, **12**, 620–628.

Maykut, G. A. and N. Untersteiner, 1971: Some results from a time-dependent thermodynamic model of sea ice. *J. Geophys. Res.*, **76**, 1550–1575.

McFarlane, N. A., 1987: The effect of orographically excited gravity-wave drag on the circulation of the lower stratosphere and troposphere. *J. Atmos. Sci.*, **44**, 1775–1800.

Miller, M. J., T. Palmer and R. Swinbank, 1989: Parameterization and influence of subgridscale orography in general circulation and numerical weather prediction models. *Meteorol. Atmos. Phys.*, **40**, 84–109.

Palmer, T. N., G. Shutts and R. Swinbank, 1986: Alleviation of a systematic westerly bias in general circulation and numerical weather prediction models through an orographic gravity wave drag parameterization. *Quart. J. Roy. Meteor. Soc.*, **112**, 1001–1039.

Phillips, T. J., 1994: Summary documentation of the AMIP models. Tech. Rep. UCRL-ID-116384, Program for Climate Model Diagnosis and Intercomparison.

Rigor, I., 2000: Variations in surface air temperature observations in the Arctic, 1979-1997. *J. Climate*, **13**, 896–914.

Steele, M. and G. M. Flato, 1999: Sea ice growth, melt, and modeling: A survey. in *The Arctic Ocean Freshwater Budget*. NATO ARW Volume, Plenum, New York, London.

Walsh, J. E. and R. G. Crane, 1992: A comparison of gcm simulations of Arctic climate. *Geophys. Res. Lett.*, **19**, 29–32.

Weatherly, J., B. P. Briegleb, W. Large and J. Maslanik, 1998: Sea ice and polar climate in NCAR CSM. *J. Climate*, **11**, 1472–1486.

Yagai, I. and K. Yamazaki, 1988: Effect of the internal gravity wave drag on the 12-layer mri gcm january simulation. in *Proc. of the WGNE Workshop on Systematic Errors in Models of the Atmosphere*. Working Group on Numerical Experimentation, Toronto, 8 pp.

Yang, J. and J. D. Neelin, 1993: Sea ice interactions with the thermohaline circulation. *Geophys. Res. Lett.*, **20**, 217–220.

Zhang, J. and W. D. Hibler III, 1997: On an efficient numerical method for modeling sea ice dynamics. *J. Geophys. Res.*, **102**, 8691–8702.

Zhang, S., C. A. Lin and R. J. Greatbatch, 1995: A decadal oscillation due to the coupling between an ocean circulation model and a thermodynamics sea-ice model. *J. Mar. Res.*, **53**, 79–106.

Zillman, J. W., 1972: A study of some aspects of the radiation and heat budgets of the southern hemisphere oceans. in *Meteoroligical Studies*, Vol. 26, p. 562. Printed by Bureau of Meteorology, Depart. of the Interior, Canberra, Australia.

Cecilia M. Bitz, Polar Science Center, University of Washington, 1013 NE 40th St., Seattle, WA, 98105

John Fyfe and Greg Flato, Canadian Centre for Climate Modelling and Analysis, Meteorological Service of Canada, University of Victoria, P.O. Box 1700, Victoria, BC V8W 2Y2, Canada

This preprint was prepared with AGU's LaTeX macros v5.01, with the extension package 'AGU^{++}' by P. W. Daly, version 1.5b from 1996/10/24.